

Turbulence in Earth's core generates large topographic torques on the mantle

Tobias G. Oliver^{†,1}, Eric G. Blackman,² John A. Tarduno,³ and Michael A. Calkins¹

¹*Department of Physics, University of Colorado, Boulder, CO 80309, USA*

²*Department of Physics and Astronomy, University of Rochester, Rochester, NY 14627*

³*Department of Earth and Environmental Sciences,
University of Rochester, Rochester, NY 14627*

Seismic and geodynamic studies indicate that the boundary between the Earth's liquid outer core and solid mantle is not spherical, but is likely characterized by topography in the form of inverted mountains and valleys that have typical amplitudes of several kilometers. One of the dynamical consequences of these deformations is that turbulent flow in the core can exert pressure torques on the mantle, thereby resulting in a transfer of angular momentum between the outer core and the mantle. Understanding this transfer of angular momentum is important for explaining variations in the Earth's rotation rate, or length of day. Whether kilometer-sized topography can explain observed variations in length of day is a longstanding question in geophysics. Here we use physical scaling arguments and a suite of state-of-the-art numerical simulations of convection in a rotating spherical shell and show that topographic torques exhibit a linear dependence on topographic amplitude and a nearly quadratic dependence on flow speeds. These results imply that topographic torques are of sufficient magnitude to explain length of day variations on annual to decadal time scales.

I. INTRODUCTION

The Earth's rotation rate, or length of day (LOD), is known to vary over a broad spectrum of frequencies, ranging from the slow, secular increase caused by tidal dissipation, to inter-annual variations resulting from the interaction between atmospheric flows and the solid crust^{24,34}. The largest amplitude temporal signals present in measurements of the LOD are the so-called sub-decadal (~ 6 yrs.) fluctuations, that are widely believed to be the result of exchanges of angular momentum between the liquid core and the solid mantle^{14,15,17}. However, the physical mechanism that allows for exchanges of angular momentum between the core and mantle is poorly constrained³⁰. The axial torques required to allow this exchange may arise from a variety of sources including pressure gradients, electromagnetic and viscous stresses at the core mantle boundary (CMB), as well as gravitational torques between the mantle and solid inner core⁴. Previous work suggests that electromagnetic torques can explain LOD if the electrical conductivity of the lower mantle is

[†]tobias.oliver@colorado.edu

sufficiently large¹³. Gravitational coupling between the inner core and mantle is also capable of producing the target torque of $10^{18}\text{N} \cdot \text{m}^{3,4}$. Pressure, or topographic, coupling occurs wherever the CMB deviates from spherical symmetry. Topographic coupling between the core and mantle is one of the least understood mechanisms, due in part to the complex techniques required to model it. To date, only a single study has used three-dimensional simulations, and this work used an approximate set of boundary conditions over a limited range of parameters²³. Towards this end, the present work examines the role of topographic coupling over a broad set of numerical experiments of rotating convection in a spherical shell in which topography is superposed onto the outer boundary. The primary goals are to test the scaling behavior of topographic torques with varying input parameters, including the rotation rate, forcing strength, and topographic amplitude, and extrapolate the findings to the conditions of the outer core.

Seismological studies report CMB topography with peak to trough amplitudes near $5\text{km}^{21,32}$. There is little overlap in the spatial structure of seismically-derived CMB topography, indicating that it is poorly constrained²⁰. Nevertheless, it is likely that CMB topography is characterized by a broad spectrum of amplitudes and wavelengths, and may therefore have a structure that is similar to the Earth’s surface⁹, albeit with a smaller amplitude. The presence of seismically slow material at the base of the mantle (e.g. the so-called Large Low Shear Velocity Provinces, or LLSVPs) below southern Africa and the southern Pacific⁸ likely contribute to deformations at the CMB which may influence flow in the outer core³³.

When deviations in spherical symmetry are present on the CMB, non-radial pressure forces will be exerted on the CMB by the outer core. Such forces can then give rise to torques on the mantle that, in turn, cause changes in its angular momentum. Predictions for Γ_z , the topographic torque about the Earth’s rotation axis, can be expressed in terms of ϵ and $\partial_\phi p$, the non-dimensional topographic amplitude and azimuthal (longitudinal) pressure gradient^{12,30}. If the pressure variations are induced by the topography, then $\Gamma_z = O(\epsilon^2)^{1,11,16,22}$. Alternatively, if the dominant contribution to the pressure gradient is not dependent on the topographic amplitude, the magnitude of the axial torque scales like $\Gamma_z = O(\epsilon)$. Given that $\epsilon \sim 10^{-3}$ at the CMB, these two scalings can yield vastly different estimates for the topographic torque. To date, no previous studies have conclusively demonstrated the existence of either scaling in a fully self-consistent convection-driven flow. Here we confirm that the linear scaling is appropriate in the core, indicating that small scale convective turbulence is capable of generating topographic torques of sufficient magnitude to explain sub-decadal LOD variations.

We address the problem of core mantle topographic coupling by employing direct numerical

simulations of convection in a rotating spherical shell in which a single topographic bump with Gaussian profile protrudes into the core; a schematic of the domain is shown in Figure 1. This choice of topography is made both for simplicity, and to ensure a rich interaction between core flows and the mantle given that a Gaussian profile is characterized by a broad spectrum of wavelengths. In the absence of topography, the dynamics of the convection are controlled by the non-dimensional Rayleigh, Ekman, and Prandtl numbers, defined by $Ra = g\alpha\Delta T d^3/\nu\kappa$, $Ek = \nu/(\Omega d^2)$, and $Pr = \nu/\kappa$, respectively. These first two parameters determine the relative influence of the buoyancy and Coriolis forces in the system, whereas the Prandtl number determines the ratio of the thermal diffusion time to the viscous diffusion time. For simplicity we set $Pr = 1$ in all simulations. The outer core is thought to be turbulent and yet strongly constrained by rotation; in this regime $Ek \rightarrow 0$ and the parameter $\widetilde{Ra} = Ek^{4/3}Ra$ plays the critical role¹⁹. Because of computational limitations, numerical simulations cannot employ the same non-dimensional parameters of the core. Rather, as is common practice⁷, our goal is to vary these parameters systematically to identify the appropriate asymptotic regime such that our findings can be extrapolated to core conditions. For the topographic bump, we fix the location and width, and vary the amplitude, ϵ . Thus, three non-dimensional control parameters are varied in this investigation.

II. METHODS

A. Governing Equations

For simplicity, the present work focuses solely on the hydrodynamic problem of convection of a Boussinesq fluid contained within a rotating spherical shell with inner radius r_{icb} and outer radius r_{cmb} . In the absence of topography the aspect ratio of the shell is fixed at $\chi = r_{icb}/r_{cmb} = 0.35$. As discussed below, finite amplitude topography is superposed onto the outer shell. The physical properties of the fluid are the kinematic viscosity ν , thermal diffusivity κ and thermal expansion coefficient α . The inner and outer boundaries are held at fixed temperatures T_{icb} and T_{cmb} , respectively. Ω is the angular rotation rate. We assume a uniform distribution of mass within the shell such that the gravitational acceleration varies linearly with radius and has magnitude g at the outer boundary. The governing equations reflect the conservation of momentum, energy, and mass and are non-dimensionalized by the shell gap-width $d = 2260\text{km}$, viscous diffusion time d^2/ν and temperature difference $\Delta T = T_{icb} - T_{cmb}$. The equations then become

$$\frac{\partial \mathbf{u}}{\partial t} + \mathbf{u} \cdot \nabla \mathbf{u} = -\nabla p + \nabla^2 \mathbf{u} - \frac{2}{Ek} \hat{\mathbf{z}} \times \mathbf{u} + \frac{Ra}{Pr} \frac{\mathbf{r}}{r_{cmb}} \vartheta \quad (1a)$$

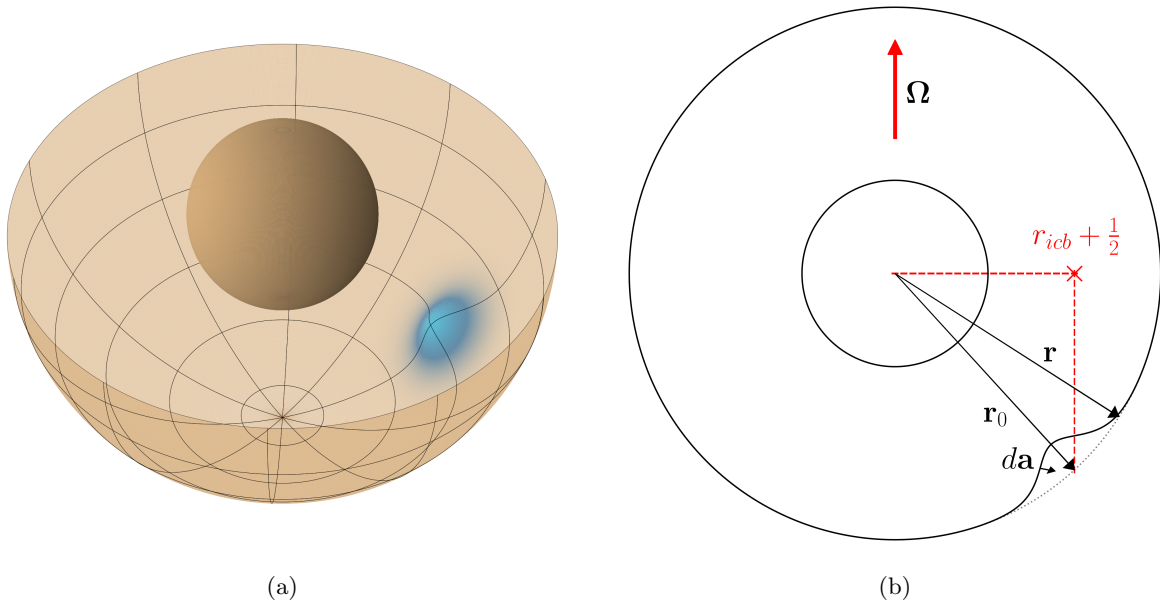


FIG. 1: Schematics of the simulation domain: (a) cut-away view of the lower hemisphere with Gaussian bump coloured in blue (no topography is present on the upper hemisphere or the inner core); (b) meridional cross-section of the domain showing the position of the bump. The rotation vector is denoted by Ω , \mathbf{r}_0 is the vector pointing from the origin to the base of the bump. The base of the bump is located below the halfway point between the inner and outer surface.

$$\frac{\partial \vartheta}{\partial t} + \mathbf{u} \cdot \nabla \vartheta = \frac{1}{Pr} \nabla^2 \vartheta \quad (1b)$$

$$\nabla \cdot \mathbf{u} = 0. \quad (1c)$$

The fluid variables are the velocity \mathbf{u} , pressure p and temperature ϑ . The non-dimensional control parameters are the Rayleigh number, Ekman number, and the thermal Prandtl number, defined by, respectively,

$$Ra = \frac{g\alpha\Delta T d^3}{\nu\kappa}, \quad Ek = \frac{\nu}{\Omega d^2}, \quad Pr = \frac{\nu}{\kappa}. \quad (2)$$

The Prandtl number is fixed to unity. No-slip, impenetrable and isothermal boundary conditions are employed on the inner and outer surfaces. The Reynolds number is a diagnostic parameter that characterizes the flow speed. We define it as

$$Re = \sqrt{\overline{\langle \mathbf{u} \cdot \mathbf{u} \rangle}}, \quad (3)$$

where the overline denotes a time average and $\langle \cdot \rangle$ indicates a volume average.

B. Topography

Given that the CMB is poorly constrained by seismology, we are motivated to use as simple a model as possible for its shape, whilst retaining the ability to easily control essential physical characteristics such as amplitude and width. In this regard we superpose a Gaussian bump on the outer boundary, as shown in Figure 1. Rotating convection in a spherical shell is known to be anisotropic and inhomogeneous, which suggests the location of the topography may also play a key role, at least insofar as the dynamical consequences of the topography on the convective flows are concerned. For the present investigation, we place the bump in the lower hemisphere at a latitude that is intended to ensure a robust interaction with time-dependent convective Rossby waves and the geostrophic, zonal flows that develop in a rotating, spherical geometry. We fix the coordinates of the center of the base of the bump such that it lies directly beneath the halfway point between inner and outer boundaries, as shown in Figure 1(b). The spherical coordinates are thus $(\theta_0, \phi_0) = (2.40, 0)$. The topographic shape function is given by

$$h(\theta, \phi) = \exp \left[-\frac{1}{\beta} \left(\frac{(\mathbf{r} - \mathbf{r}_0)^2}{r_{cmb}^2} \right) \right], \quad (4)$$

with \mathbf{r}_0 the vector pointing from the origin to $(r_{cmb}, \theta_0, \phi_0)$. The topographic amplitude is ϵ and β denotes a measure of the width (lateral extent) of the topography. We fix the width in this study such that $\beta^{-1} = 40$. As mentioned in previous work⁵, the Gaussian profile is particularly useful since its representation in spectral space requires a broad range of spherical harmonics, and therefore lends the possibility of richer dynamical interactions with the convective flow field.

The simulations are performed with the computational fluid dynamics code `Nek5000`¹⁰, which uses the spectral element method²⁹ and therefore easily allows for solving the governing equations in domains with irregular boundaries. `Nek5000` has been extensively benchmarked and scales efficiently to large numbers of processors. The simulations were run on up to 2048 processors for our most demanding simulations. `Nek5000` uses a CFL condition to dynamically update the timestep. Our tests indicate that for identical non-dimensional control parameters the `Nek5000` code is approximately a factor of ten slower in comparison to the commonly used spectral code, `Rayleigh`²⁶, although spectral codes are generally incapable of handling irregular boundaries. All simulations used a degree 7 polynomial interpolant within the spectral elements. The most demanding simulations required 331,776 spectral elements, corresponding to almost 1.7×10^8 physical grid points.

C. Choice of parameter values

Core turbulence is thought to be strongly constrained by the effects of the Coriolis force. Thus, our present goal is to model convection in this rotationally constrained regime while simultaneously allowing for as broad a range of spatiotemporal scales as is numerically feasible. Moreover, as is often done in studies of core dynamics, it is important to understand how the dynamics of the system change as the parameters are made more extreme. We therefore cover a broad range in Rayleigh number and Ekman number in an effort to elucidate the scaling behavior of the dynamics. Our simulations use Ekman numbers of $Ek = [10^{-6}, 3 \times 10^{-6}, 10^{-5}, 3 \times 10^{-5}, 10^{-4}]$ and reduced Rayleigh numbers of $\widetilde{Ra} = [3, 10, 20, 40, 60]$.

Concerning the choice of topographic parameters, the present work is focused predominantly on how the topographic torque and associated convective dynamics depend on the amplitude, ϵ . Although seismic studies and mantle convection simulations indicate that CMB topography amplitudes are unlikely to exceed $\epsilon = O(10^{-3})$, it makes little sense to use amplitudes this small given that the investigated range of Ekman numbers in our simulations is so distant from the Earth's core. Indeed, using such a value in our simulations would confine the topography within the Ekman boundary layer present on the outer surface of the simulation domain. It is well known that the influence of the bounding surface is thought to become more important dynamically as the Ekman number decreases. Therefore we perform simulations at $\epsilon = 0.2$ and limited sweeps across $\epsilon = [0.005, 0.01, 0.02, 0.03, 0.05, 0.1, 0.2, 0.3]$.

D. Topographic Torques

The topographic torque is defined by

$$\mathbf{\Gamma} = \oint \mathbf{r} \times p \, d\mathbf{a}, \quad (5)$$

where \mathbf{r} is the position vector pointing from the center of the planet to the surface of the CMB, p is pressure and $d\mathbf{a}$ is a surface area element of the CMB pointing away from the core. In this study we allow for deviations from spherical symmetry and denote the radial position of the CMB as $r = r_{cmb} [1 - \epsilon h(\theta, \phi)]$, where r_{cmb} is the non-dimensional radius of the CMB in the absence of topography, ϵ is the topographic amplitude and $h(\theta, \phi)$ is defined by equation 4. Insight into how this deviation influences torques can be gained by assuming $\epsilon \ll 1$ such that the component of $\mathbf{\Gamma}$

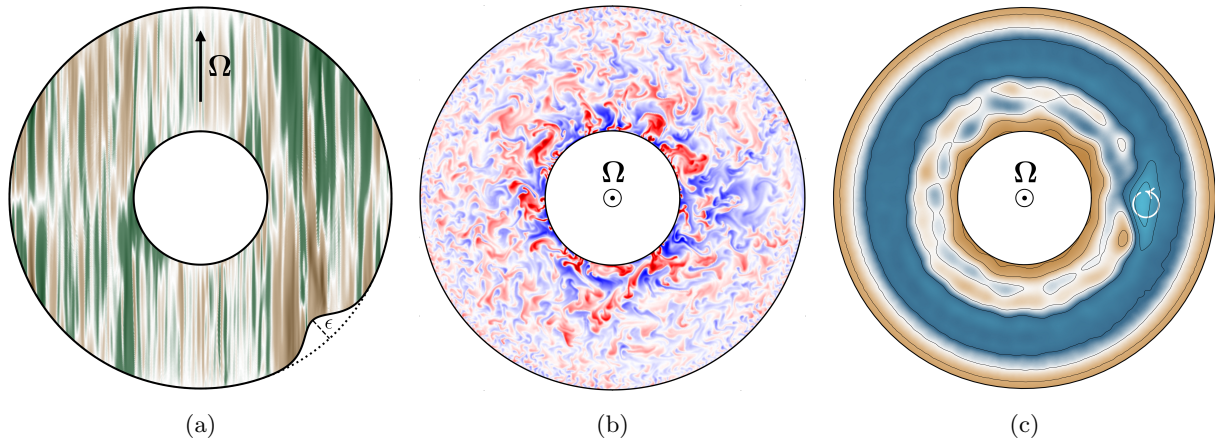


FIG. 2: Flow visualizations for $Ek = 10^{-6}$, $\widetilde{Ra} = 60$, and $\epsilon = 0.2$: (a) meridional cross-section of the instantaneous vertical velocity; (b) equatorial cross-section of the instantaneous temperature field with the conductive profile and zonal-average removed. (c) Time- and depth-averaged pressure. Blue (brown) corresponds to pressure lows (highs). The circular arrow in (c) indicates the direction of the cyclonic flow over the bump.

in the direction of the Earth's rotation axis can be written as³⁰

$$\Gamma_z \approx \epsilon \oint h(\theta, \phi) \partial_\phi p \, da. \quad (6)$$

The above relation shows that when the dominant contribution to the pressure gradient is not dependent on the topographic amplitude, the magnitude of the axial torque scales like $\Gamma_z = O(\epsilon)$. Alternatively, if the dominant contribution to the pressure gradient arises as a perturbation to an otherwise uniform (zero pressure gradient) flow, then we have $\partial_\phi p = O(\epsilon)$ and therefore $\Gamma_z = O(\epsilon^2)$ ^{1,11,16,22}.

The time-dependent topographic torque on the CMB is computed directly from equation (5); we do not use the small amplitude approximation of this integral. In the present work we focus on the axial component of the topographic torque only, Γ_z . The time average and standard deviation of Γ_z are calculated. For the sake of notational simplicity, they are denoted $\bar{\Gamma}_z$ and Γ'_z respectively.

III. RESULTS

Visualizations of the flow field are shown in Figure 2 for the most extreme rotation rate ($Ek = 10^{-6}$), with $\widetilde{Ra} = 60$ and $\epsilon = 0.2$. Meridional slices show the presence of columnar convection structures that effectively span the entire local depth of the domain. These structures drift with

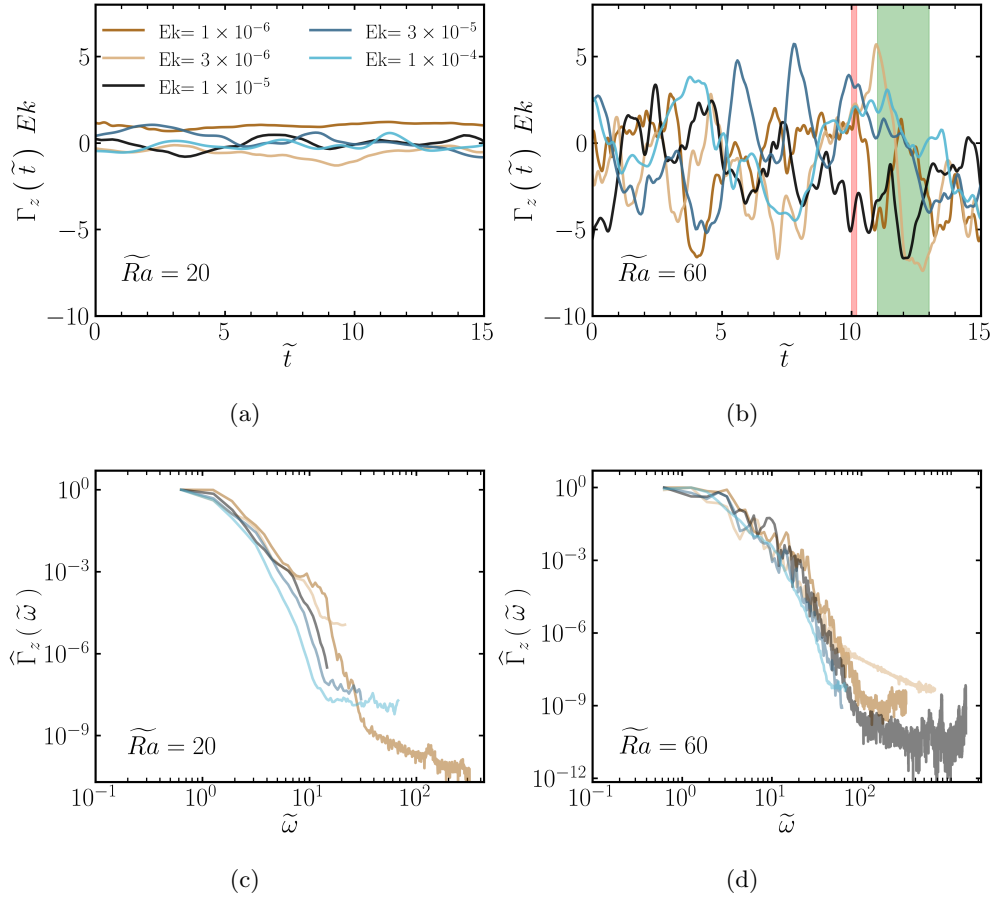


FIG. 3: (Top row) Time series of the torque and (bottom row) the corresponding periodograms of the torque for $\epsilon = 0.2$. Left $\tilde{Ra} = 20$ and right $\tilde{Ra} = 60$ for all Ek . Red and green bars in (b) correspond to decadal and centenary timescales respectively.

time and directly interact with the CMB topography. This view, along with equatorial slices, show the hallmark of turbulent rotating spherical convection: strong mixing in planes perpendicular to the rotation axis, yet approximately invariant parallel to the rotation axis. The dynamical effects of the topography are present in these snapshots of the flow – Figure 2(b), where we find subdued mixing in the column extending axially from the bump with locally cold fluid indicated by the predominantly blue color. Further evidence that this bump impacts the dynamics of the core is found in the time- and axially-averaged pressure field shown in Figure 2(c); a steady, cyclonic gyre is observed directly above the topography.

Time series and corresponding periodograms of the topographic torque are shown in Figure 3 for $\tilde{Ra} = 20$ and 60 and all values of Ek . In the rapidly rotating regime, we expect the temporal dynamics to be dominated by the convective Rossby waves. In our non-dimensional units, these

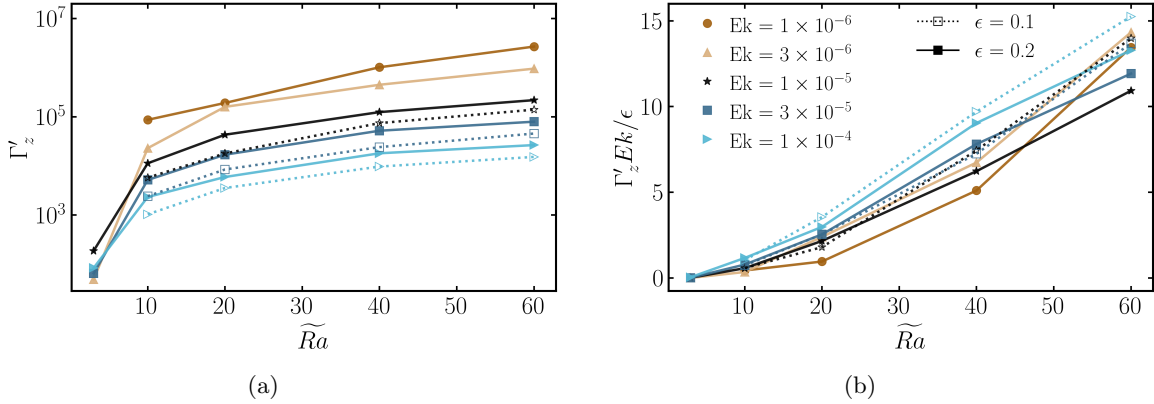


FIG. 4: Topographic torque versus reduced Rayleigh number $\tilde{Ra} = RaEk^{4/3}$: (a) raw (unscaled) data and (b) axial torque scaled by Ek/ϵ .

waves have angular frequencies that vary as $\omega \sim Ek^{-2/3}$ ¹⁸. Thus, in order to meaningfully compare the simulations at different rotation rates, the data is plotted against the rescaled time and frequency, $\tilde{t} = Ek^{-2/3}t$ and $\tilde{\omega} = Ek^{2/3}\omega$, respectively. The periodograms are an estimate of the spectral density and are calculated with Welch's method³⁵ over a Hann window of size $\tilde{t} = 10$. Here we observe that in these rescaled units the simulations are characterized by similar time scales, showing that the asymptotic state relevant for understanding core dynamics is present in the models. As \tilde{Ra} is increased the amplitude of the fluctuations increase, as does the temporal complexity. However, the periodograms do not differ significantly between different \tilde{Ra} , suggesting the increased complexity at higher \tilde{Ra} is restricted to smaller amplitude fluctuations.

Under Earth-like conditions, a decadal timescale corresponds to $\tilde{t} \approx 0.2$ (see Appendix, Section A). The red shaded region in Figure 3(c) corresponds to $\tilde{t} = 0.2$ while the green shaded region corresponds to $\tilde{t} = 2.0$. Although our current data suggests that fluctuations take place on a timescale closer to 100 years, the simulations are far less turbulent than the expected conditions of the core; accepted values of flow speeds for the core are at least five orders of magnitude greater than the simulated values. As the forcing is increased and the flow becomes more turbulent, the advective timescales are known to decrease, and this behavior is also observed in the simulations.

The standard deviation of the axial topographic torque (Γ'_z) is computed for all simulations and plotted in Figure 4(a). Dashed (solid) lines with open (solid) symbols correspond to $\epsilon = 0.1$ ($\epsilon = 0.2$). For a fixed topographic amplitude we observe an increase in Γ'_z as Ek is reduced, showing that CMB topography has a stronger influence on core flows as the rotation rate increases. We emphasize that the abscissae are the reduced quantity \tilde{Ra} . In dimensional terms this means that as

the Coriolis force is increased, so too is the buoyancy force so that the flow remains super-critical. We also find that Γ'_z increases as \widetilde{Ra} is increased, demonstrating that larger pressure gradients develop within the flow as the buoyancy force is increased. Insight into the dependence of the torque on Ek is sought in the asymptotic theory for rotating spherical convection²⁷. Over our investigated range of parameters we expect the flow to be quasi-geostrophic in the sense that the Coriolis force and pressure gradient force are approximately balanced,

$$\frac{2}{Ek} \hat{\mathbf{z}} \times \mathbf{u} \approx -\nabla p. \quad (7)$$

In our non-dimensional units, geostrophy occurs on a $O(Ek^{1/3})$ length scale such that $\nabla \sim Ek^{-1/3}$ and the velocity field scales as $\mathbf{u} = O(Ek^{-1/3})$. Thus, the geostrophic balance given above implies

$$p = O(Ek^{-1}) \quad \Rightarrow \quad \Gamma'_z = O(Ek^{-1}). \quad (8)$$

For simplicity we refer to the quantity $\Gamma'_z Ek$ as the reduced torque; a plot is shown in the Extended Data Figure E.1(a). The reduced torque is order unity across the entire range of parameters investigated and is separated into two distinct branches corresponding to $\epsilon = 0.1$ and $\epsilon = 0.2$. To determine how the torque depends on topographic amplitude we rescale the reduced torque by ϵ as shown in Figure 4(b). Good collapse of the data is observed, although there remains a strong dependence on \widetilde{Ra} . Rescaling the torques by Ek/ϵ^2 yields values that are no longer order unity and there is significant separation in the data corresponding to different amplitudes which is strongly suggestive that a scaling of $\Gamma'_z \sim \epsilon^2$ is not represented by our data (see Figure E.1(b)).

Further testing of the amplitude dependence is carried out by varying ϵ for Ekman numbers $Ek = [10^{-5}, 3 \times 10^{-6}]$ and fixed $\widetilde{Ra} = 40$. Figure 5(a) shows the computed reduced torque for these cases. A least squares power law fit to the data yielded $\Gamma'_z Ek = 7.7\epsilon^{1.07}$, and is shown by the dashed line. Slopes of ϵ and ϵ^2 are shown for reference. These results provide further evidence that the topographic torque scales linearly with topographic amplitude, as would be expected if the primary component of the pressure that contributes to the torque is that associated with the convection (i.e. the pressure is, to leading order, not dependent on ϵ).

To extrapolate our findings to the conditions of the core, we require the functional dependence $\Gamma'_z = f(\widetilde{Ra})$, or, alternatively, $\Gamma'_z = g(Re)$, for some functions f and g . Rescaling the torque by $\epsilon \widetilde{Ra}^2$ produces a reasonable collapse of the data (see supplementary figure E.2), although the \widetilde{Ra} -dependence appears to become stronger as Ekman is reduced. Admittedly, our data represents a limited range of parameter space, and it is possible that there is no simple power law scaling for $f(\widetilde{Ra})$. Previous studies suggest that the small scale Reynolds scales approximately as $ReEk^{1/3} \sim$

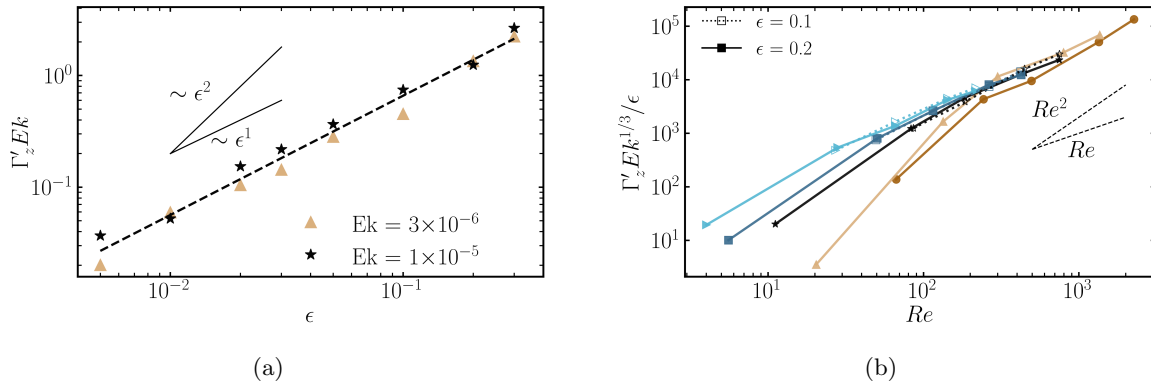


FIG. 5: (a) Reduced topographic torque versus topographic amplitude (ϵ) for $\widetilde{Ra} = 40$ and $Ek = (3 \times 10^{-6}, 10^{-5})$. A least squares fit of the data gives a scaling of $\Gamma'_z Ek = 7.7\epsilon^{1.07}$ shown with the dashed line. Linear and quadratic scalings in ϵ are shown for reference. (b) Topographic torque scaled by $Ek^{1/3}/\epsilon$ as a function of flow speeds (Re). The data appears to collapse well and looks to be approaching a Re^2 scaling for the largest Re (lowest Ek).

\widetilde{Ra} , as \widetilde{Ra} becomes large^{25,27,28}. The quantity $\Gamma'_z Ek^{1/3}/\epsilon$ is plotted against Re in Figure 5(b). With the exception of the lowest \widetilde{Ra} simulations in which the flow is very close to onset and is dominated by a few oscillatory modes, the data collapses well. With our current dataset it is difficult to recover a scaling relationship for Re , although for our most turbulent (smallest Ek) simulations, it appears that Γ'_z is approaching $\sim Re^2 \epsilon Ek^{-1/3}$. The presence of this quadratic dependence on flow speed is reminiscent of form drag in non-rotating hydrodynamics, so may not be unexpected here.

IV. DISCUSSION

The significance that topographic torques play in explaining the sub-decadal fluctuations in the LOD has been debated for more than 50 years¹². This debate, which is centered on two competing hypotheses, has focused on how the torques depend on the typical amplitude of the topography. It is known that a non-axisymmetric pressure gradient is required to generate non-trivial axial torques on the mantle. The first hypothesis assumes that the flow in the core is predominantly axisymmetric and the topography induces the necessary non-axisymmetric pressure gradients¹. Models using this hypothesis yield topographic torques that scale quadratically with the topographic amplitude. The second hypothesis considers the convection to be the dominant source of asymmetry such that the pressure gradients do not depend on topographic amplitude to leading order, which leads to a linear

scaling. Our investigation has shown that this second mechanism dominates when convection is considered in the problem – convection-driven waves with angular frequency $\omega \sim Ek^{-2/3}$, which are inherently non-axisymmetric, yield pressure gradients that interact with the topography to produce a torque that is linearly proportional to the topographic amplitude.

The results also show that the topographic torque scales nearly quadratically with the flow speeds at the most extreme parameter values accessed in the simulations. This scaling is nearly consistent with the classical picture of ‘form drag’ that occurs in turbulent flows, although rotation appears to play an additional role via the factor of $Ek^{-1/3}$. This ‘additional’ Ekman number dependence suggests that torque is dependent not only on flow speeds, but also the spatial structure of the underlying convection, which is controlled by the importance of rotation through the Ekman number. Thus, our investigation shows that an approximate scaling of the topographic torque is given by $\Gamma'_z \sim \epsilon Re^2 Ek^{-1/3}$. We note that the flow speed, and therefore the Reynolds number, is not independent of Ek . For instance, it is known that when the system is strongly forced by fixed temperature boundary conditions, the Reynolds number scales approximately like $Re \sim EkRa/Pr$ and the singularity as $Ek \rightarrow 0$ is avoided²⁸. Thus, our derived torque scaling should be understood to depend on all of the control parameters.

The dimensional torques required to explain observed sub-decadal LOD variations are nearly 10^{18} N·m³⁰. In dimensional form our scaling becomes

$$\Gamma'_{z, \text{dim}} \sim \rho \epsilon U^2 d^3 Ek^{-1/3}, \quad (9)$$

where U is a characteristic flow speed and fluid density is denoted by ρ . Using estimates for the outer core we have $\rho \sim 10^4 \text{kg/m}^3$, $\epsilon \sim 10^{-3}$ (corresponding to an amplitude of 2.26 km), $U = (1 - 5) \times 10^{-4}$ m/s, $d = 2260$ km, and $Ek = 10^{-15}$. These values give a dimensional torque of $(1.2 \times 10^{17} - 2.9 \times 10^{18})$ N·m, which is consistent with the required torques.

Magnetism and global scale topography likely also play a role in controlling LOD. However, because the primary flow quantities, such as flow speeds, show similar scaling behavior in simulations of both dynamos and convection^{6,27}, the scaling of the topographic torques are unlikely to change fundamentally when magnetism is introduced. Thus, based on our state-of-the-art numerical simulations of convection in a rotating spherical shell, we conclude that kilometer-sized CMB topography can explain sub-decadal LOD variations.

V. APPENDIX

A. Relating \tilde{t} to length of day

The rescaled time \tilde{t} can be related to the length of day as follows. Denoting dimensional time (in seconds) as τ we have

$$\tilde{t} = Ek^{-2/3} \left(\frac{\nu}{d^2} \right) \tau = Ek^{1/3} \left(\frac{\nu}{d^2} \right) \left(\frac{\Omega d^2}{\nu} \right) \tau = Ek^{1/3} \Omega \tau. \quad (\text{A.1})$$

We note that \tilde{t} should be considered as a small scale diffusion time. From the linear stability analysis $\ell/d = Ek^{1/3}$ where ℓ is the length scale associated with the convection at onset. Even in the turbulent regime, the flow structures, such as the thickness of the Taylor columns, may remain $O(Ek^{1/3})^{27,28}$. Therefore,

$$\tilde{t} = \left(\frac{\nu}{\ell^2} \right) \tau. \quad (\text{A.2})$$

Plugging in $Ek = 10^{-15}$ and $\Omega = 7.27 \times 10^{-5} \text{ s}^{-1}$ into Equation (A.1) gives

$$\tilde{t} = 7.27 \times 10^{-10} \tau. \quad (\text{A.3})$$

A decadal timescale corresponds to $\tau \approx 3 \times 10^8 \text{ s}$ such that

$$\tilde{t} \approx 0.2. \quad (\text{A.4})$$

-
- [1] ANUFRIEV, A. P. & BRAGINSKY, S. I. 1977 Influence of irregularities of the boundary of the Earth's core on the velocity of the liquid and on the magnetic field, III. *Geomagn. & Aeron.* **17**, 492–496.
 - [2] BOERNER, T. J., DEEMS, S., FURLANI, T. R., KNUTH, S. L. & TOWNS, J. 2023 Access: Advancing innovation: NSF's advanced cyberinfrastructure coordination ecosystem: Services & support. In *Practice and Experience in Advanced Research Computing*, pp. 173–176. New York, NY, USA: ACM.
 - [3] BUFFETT, B.A., MOUND, J. & JACKSON, A. 2009 Inversion of torsional oscillations for the structure and dynamics of Earth's core. *GJI* **177**, 878–890.
 - [4] BUFFETT, BRUCE A. 1996 Gravitation oscillations in the length of the day. *Geophys. Res. Letters* **23** (17), 2279–2282.
 - [5] CALKINS, M. A., NOIR, J., ELDREDGE, J. D. & AURNOU, J. M. 2012 The effects of boundary topography on convection in Earth's core. *GJI* **189**, 799–814.
 - [6] CALKINS, M. A., ORVEDAHL, R. J. & FEATHERSTONE, N.A. 2021 Large-scale balances and asymptotic scaling behaviour in spherical dynamos. *GJI* **227**, 1228–1245.

- [7] CHRISTENSEN, U. 2010 Dynamo scaling laws and applications to the planets. *Space Sci. Rev.* **152**, 565–590.
- [8] COTTAAR, SANNE & LEKIC, VEDRAN 2016 Morphology of seismically slow lower-mantle structures. *Geophysical Supplements to the Monthly Notices of the Royal Astronomical Society* **207** (2), 1122–1136.
- [9] ERMAKOV, AI, PARK, RS & BILLS, BG 2018 Power laws of topography and gravity spectra of the solar system bodies. *J. Geophys. Res.: Planets* **123** (8), 2038–2064.
- [10] FISCHER, PAUL, KERKEMEIER, STEFAN & ET. AL. 2019 Nek5000 version 19.0.
- [11] GLANE, SEBASTIAN & BUFFETT, BRUCE 2018 Enhanced core-mantle coupling due to stratification at the top of the core. *Frontiers in Earth Science* **6**, 171.
- [12] HIDE, R. 1969 Interaction between the Earth’s liquid core and solid mantle. *Nature* **222**, 1055–1056.
- [13] HOLME, RICHARD 1997 Electromagnetic core-mantle coupling–I. explaining decadal changes in the length of day. *GJI* **132**, 167–180.
- [14] HOLME, R. 2015 Large scale flow in the core. In *Treatise on Geophysics* (ed. G. Schubert), , vol. 8, pp. 107–130. Elsevier.
- [15] JACKSON, A., BLOXHAM, J. & GUBBINS, D. 1993 Time-dependent flow at the core surface and conservation of angular momentum in the coupled core-mantle system. *Dynamics of Earth’s Deep Interior and Earth Rotation* **72**, 97–107.
- [16] JAULT, DOMINIQUE 2020 Tangential stress at the core–mantle interface. *GJI* **221** (2), 951–967.
- [17] JAULT, D., GIRE, C. & MOUËL, J. L. LE 1988 Westward drift, core motions and exchanges of angular momentum between core and mantle. *Nature* **333**, 353–356.
- [18] JONES, C. A., SOWARD, A. M. & MUSSA, A. I. 2000 The onset of thermal convection in a rapidly rotating sphere. *J. Fluid Mech.* **405**, 157–179.
- [19] JULIEN, K., RUBIO, A. M., GROOMS, I. & KNOBLOCH, E. 2012 Statistical and physical balances in low Rossby number Rayleigh–Bénard convection. *Geophys. Astrophys. Fluid Dyn.* **106** (4-5), 392–428.
- [20] KOELEMELJER, P. 2021 Toward consistent seismological models of the core–mantle boundary landscape. *Mantle convection and surface expressions* pp. 229–255.
- [21] KOPER, KEITH D., PYLE, MOIRA L. & FRANKS, JILL M. 2003 Constraints on aspherical core structure from PKiKP–PcP differential travel times. *J. Geophys. Res.: Solid Earth* **108** (B3), arXiv: <https://agupubs.onlinelibrary.wiley.com/doi/pdf/10.1029/2002JB001995>.
- [22] KUANG, W. J. & BLOXHAM, J. 1993 The effect of boundary topography on motions in the Earth’s core. *Geophys. Astrophys. Fluid Dyn.* **72**, 161–195.
- [23] KUANG, W. J. & CHAO, B. F. 2001 Topographic core-mantle coupling in geodynamo modeling. *Geophys. Res. Letters* **28** (9), 1871–1874.
- [24] LAMBECK, KURT 2005 *The Earth’s variable rotation: geophysical causes and consequences*. Cambridge University Press.
- [25] MAFFEI, S., KROUSS, M. J., JULIEN, K. & CALKINS, M. A. 2021 On the inverse cascade and flow speed scaling behaviour in rapidly rotating Rayleigh–Bénard convection. *J. Fluid Mech.* **913**, A18.

- [26] MATSUI, H. & OTHERS 2016 Performance benchmarks for a next generation numerical dynamo model. *Geochem. Geophys. Geosyst.* **17**, 1586–1607.
- [27] NICOSKI, J A, O’CONNOR, A R & CALKINS, M A 2024 Asymptotic scaling relations for rotating spherical convection with strong zonal flows. *J. Fluid Mech.* **981**, A22.
- [28] OLIVER, T., JACOBI, A., JULIEN, K. & CALKINS, M.A. 2023 Small scale quasigeostrophic convective turbulence at large rayleigh number. *Phys. Rev. Fluids* p. 093502.
- [29] PATERA, T.A. 1984 A spectral element method for fluid dynamics : laminar flow in a channel expansion. *J. of Comp. Phys.* **54**, 468–488.
- [30] ROBERTS, P. H. & AURNOU, J. M. 2012 On the theory of core-mantle coupling. *Geophys. Astrophys. Fluid Dyn.* **106** (2), 157–230.
- [31] STANZIONE, D., WEST, J., EVANS, R. T., GHATTAS, O. & DHABALESWAR, K. P. 2020 Frontera: The evolution of leadership computing at the national science foundation. *Practice and Experience in Advanced Research Computing (PEARC ’20)* .
- [32] TANAKA, S. 2010 Constraints on the core-mantle boundary topography from P4KP-PcP differential travel times. *J. Geophys. Res.* **115** (B04310).
- [33] TARDUNO, JOHN A, WATKEYS, MICHAEL K, HUFFMAN, THOMAS N, COTTRELL, RORY D, BLACKMAN, ERIC G, WENDT, ANNA, SCRIBNER, CECILIA A & WAGNER, COURTNEY L 2015 Antiquity of the South Atlantic Anomaly and evidence for top-down control on the geodynamo. *Nat. Comm.* **6** (1), 7865.
- [34] WAHR, JOHN M. 1988 The Earth’s rotation. *Annu. Rev. Earth Planet. Sci.* **16** (231-249).
- [35] WELCH, P.D. 1967 The use of fast Fourier transform for the estimation of power spectra: a method based on time averaging over short, modified periodograms. *IEEE Trans. on Audio and Electroacoustics* **15**, 70–73.

VI. END NOTES

Acknowledgements

This work was funded by the National Science Foundation through CSEDI grant EAR-2201595. The Stampede3 and Anvil supercomputers at the Texas Advanced Computing Center (TACC) and Purdue University, respectively, were made available through allocation PHY180013 from the Advanced Cyberinfrastructure Coordination Ecosystem: Services & Support (ACCESS) program, which is supported by National Science Foundation grants #2138259, #2138286, #2138307, #2137603, and #2138296². Access to the Frontera supercomputer³¹ at TACC was made available through grant EAR24006. This work also utilized the Alpine high performance computing resource at the University of Colorado Boulder. Alpine is jointly funded by the University of

Colorado Boulder, the University of Colorado Anschutz, and Colorado State University.

TGO prepared and performed the simulations. TGO and MAC prepared the text and figures. JAT and EGB provided insight and assisted with text preparation.

Extended Data is available for this paper.

Correspondence and requests for materials should be addressed to Tobias Oliver (tobias.oliver@colorado.edu).

Presented data is made publicly available at

https://github.com/tgoliver/TGO_Topographic_Coupling_Data

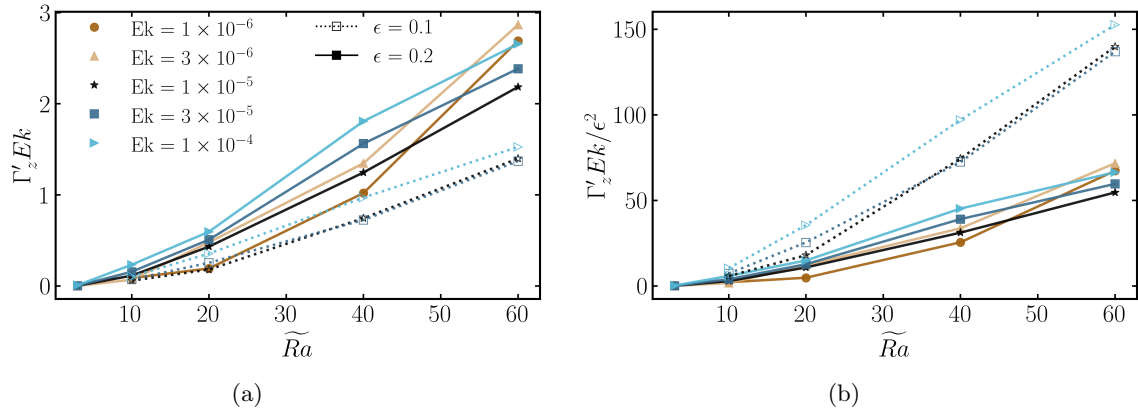


FIG. E.1: Topographic torque versus reduced Rayleigh number $\widetilde{Ra} = RaEk^{4/3}$ for various scalings: (a)-(b) axial torque scaled by Ek and Ek/ϵ^2 respectively.

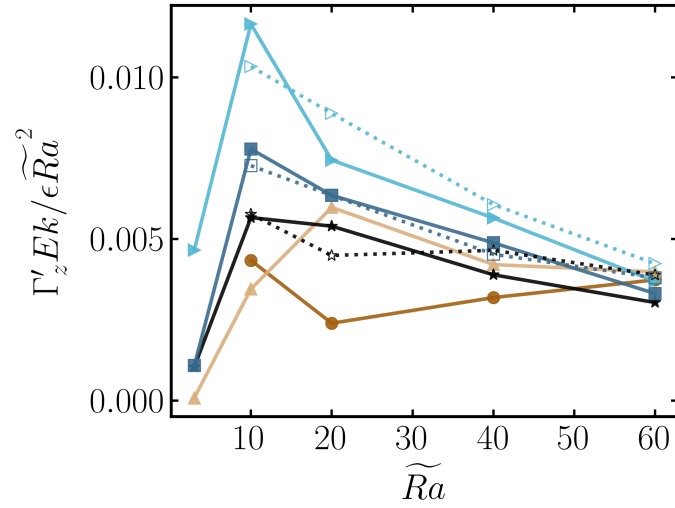


FIG. E.2: Scaled topographic torque as a function of thermal forcing (\widetilde{Ra}).

VII. EXTENDED DATA